Electric-field-induced phase transitions in frustrated cholesteric liquid crystals of negative dielectric anisotropy

P. Ribière, S. Pirkl,* and P. Oswald

*Ecole Normale Supérieure de Lyon, Laboratoire de Physique, 46 Allée d'Italie,
69364 Lyon CEDEX 07, France*

The phase diagram of a large-pitch cholesteric liquid crystal sandwiched between two parallel glass plates with homeotropic anchoring is determined both experimentally and theoretically. Contrary to previous experiments [P. Ribière and P. Oswald, J. Phys. (Paris) **51**, 1703 (1990)], the materials chosen have a negative dielectric anisotropy so that experiments are performed at smaller thickness than the critical value d_c that is necessary to unwind the helical structure completely at vanishing electric field. The two control parameters are the frustration ratio d/p of the thickness over the quiescent pitch of the cholesteric liquid crystal and the applied voltage V. The main difference with previous experiments is that the cholesteric-nematic phase transition can be second order or first order depending on the sample thickness. There is thus a Landau tricritical point in the phase diagram. Furthermore, we have found a triple point where the nematic phase coexists with both a translationally invariant configuration and a periodic structure. A theoretical model, including two order parameters, allows us to calculate the coordinates of these two particular points as a function of the Frank elastic constants as well as the general aspect of the phase diagram. The agreement between theory and experiment is satisfactory.

PACS number(s): 61.30.Gd, 64.70.Md

I. INTRODUCTION

A cholesteric phase is a nematic liquid crystal that is twisted in a single direction. Although the cholesteric and the nematic phases are not thermodynamically distinct, it is possible to induce the cholesteric-nematic phase transformation at a constant temperature by subjecting the cholesteric to an electric field or a topological frustration [1–8]. This so-called unwinding transition has been studied in detail recently, particularly with materials of positive dielectric anisotropy when the anchoring of the molecules on the limiting glass plates is homeotropic (molecules perpendicular to the surfaces). The control parameters are then the dimensionless frustration ratio $\mathcal{C} = d/p$, where d is the sample thickness and p the cholesteric pitch, and the applied voltage V (or the electric field $E = V/d$). For simplicity, we assume that $\mathcal{C} > 0$ in the following. This experiment can be performed between two parallel glass plates or in a wedge-shaped electro-optic cell. In this latter case, the sample thickness variation makes it difficult to determine precisely the phase diagram in the $(\mathcal{C}, V)$ parameter space. We have thus preferred working between two parallel glass plates. The experimental setup utilized has been described in detail in Ref. [6]. It allows us to change continuously the sample thickness with an accuracy of ± 0.05 μm while keeping the parallelism between the two semitransparent electrodes smaller than 2×10^{-4} rad.

With materials of positive dielectric anisotropy ($\epsilon_a > 0$), the molecules tend to align along the electric field. In this case, three types of solutions have been observed experimentally, depending on the values of $\mathcal{C}$ and V. If the sample is sufficiently thin, the cholesteric unwinds completely at vanishing electric field when $d < d_c$, leading to a homeotropic nematic phase. If the sample is thick enough and the electric field not too large, then cholesteric fingers occur, which can be either isolated or arranged periodically. Finally, a transient translationally invariant configuration (denoted by TIC in the following) can be observed by "quenching" the system below its spinodal limit. One knows that the order of this transition depends crucially on the elastic anisotropy of the materials, a result that has been proved theoretically [6,9]. Until now, all the materials of positive dielectric anisotropy used have led to a first-order phase transition. This result is a consequence of their anisotropy, which is in general too large (according to the theory) to observe a second-order phase transition.

In this paper we describe the phase diagram for cholesterics of negative dielectric anisotropy. In this case, the molecules orient themselves perpendicular to the electric field. As in previous experiments, we have chosen to work in homeotropic anchoring. On the other hand, experiments are performed below the unwinding threshold (at vanishing electric field) of the cholesteric phase, i.e., at $d < d_c$. In this case, it is, however, possible to recover a chiral structure by applying an electric field. Contrary to previous experiments, we shall see experimentally that the order of the transition can change depending on the sample thickness. In particular, we shall show that there exist both a triple and a tricritical point in the phase diagram. In order to explain this unexpected richness of the phase diagram, we shall generalize our previous theoretical model by including two order parameters.

The plan of this paper is then as follows: in Sec. II we describe the materials used and the sample preparation. In Sec. III the different solutions encountered are briefly

pictured as well as their main geometrical characteristics. The principle of the mapping to the unit sphere S^2 is recalled. Section IV is devoted to the determination of the experimental phase diagram. Finally, Sec. V is an extension of the model of Refs. [6] and [9] that will allow us to predict, among other things, the position of both the tricritical and the triple point in the phase diagram.

II. SAMPLE PREPARATION

Cholesteric liquid crystals of large pitch are prepared by adding a small amount of the chiral molecule S811 (from Merck Corp.) to the nematic mixtures ZLI 2806 (Merck) and Roche 2860 (Hoffmann La Roche). A few basic parameters of these mixtures are listed in Table I.

The Frank constants K_i are given for the nematic mixtures. They can be a priori slightly different in the presence of a small amount of chiral molecules. ϵ_a is the dielectric anisotropy, Δn the birefringence and K_1 (respectively, K_2, K_3) the splay (respectively twist, bend) elastic constants (from Merck and Hoffmann La Roche data).

The natural unconstrained pitch p of these two mixtures was measured using the conventional Cano wedge method. The critical sample thickness d_c at which the helical structure completely unwinds was measured in a wedge-shaped cell whose surfaces have been treated with lecithin [7,8].

We refer to Ref. [6] for a detailed description of our experimental setup. We only mention that the electrodes have been coated with silane ZLI 3124 (Merck) in order to obtain strong homeotropic alignment and that a square wave ac voltage (5 kHz) was used in order to repress the electrohydrodynamics effects.

III. DIFFERENT TYPES OF SOLUTIONS AND TOPOLOGICAL REPRESENTATION

As in previous experiments, we have observed three types of solutions. Each of them can be described by considering its image onto the unit sphere S^2. The principle of this mapping is to associate a trajectory in the real space with a trajectory on the sphere [6,9,10]. Thus, the homeotropic nematic configuration is represented by a point on the sphere, for instance the North Pole [Fig. 1(a)]. Another configuration is the TIC [Fig. 2(a)]: contrary to previous experiments on dielectrically positive materials, this configuration can be stable and not simply transient. In the case of this solution, the image of any straight line perpendicular to the glass plates is a closed loop passing through the North Pole on the sphere [Fig. 1(b)]. This condition ensures that the molecules are homeotropically anchored on the limiting glass plates.

So far, we have assumed that this curve was a circle. We have shown too that the nematic-TIC phase transition could be described satisfactorily by taking as order parameter the angle between the axis of revolution of this circle and the south-north axis of the sphere. We shall see in Sec. V that this is only an approximation. Finally, we have observed fingers that can be isolated or arranged side by side periodically [Figs. 2(b)–2(d)]. These fingers correspond to a double-twist configuration that can be described by a set of circles on the sphere. We have chosen circles for simplicity but this is an approximation. Each of them is the image of a straight line parallel to the glass plates and perpendicular to the finger axis. If the finger is bounded by homeotropic nematic, all these circles must pass through the North Pole. This condition is not fulfilled in general, so we do not assume that the circles pass through the North Pole. By contrast, the centers of these circles lie on a closed curve that always passes through the North Pole in order to fulfill the condition of homeotropic anchoring on the glass plates [Fig. 1(c)]. As for the TIC, we shall see in Sec. V that this curve is not necessarily a circle, an assumption that we previously made in Ref. [6]. This result does not change the topological properties of the fingers nor their rules of association [5,6]. In particular, an isolated finger has two different ends, one of them being sharper than the other. Two different ends can collapse whereas two identical ends always repel. Furthermore, a sharp fingertip can collapse into the side of a finger and forms a T-like side-branching, whereas a rounded tip is always repelled by the side of a finger. The rounded tips have been called normal tips because the twist inside has the same sign everywhere as that of the spontaneous twist of the free cholesteric phase. By contrast, there is a region where the twist changes sign in the sharp tips, which are called for this reason abnormal tips. In Ref. [6] we have shown that all these properties can be qualitatively explained by the topological model used here.

IV. EXPERIMENTAL PHASE DIAGRAM

In order to establish the phase diagram in the $(\mathcal{C}, V)$ plane, we first measured the unwinding critical thickness d_c (at zero electric field) by slowly decreasing the sample thickness until the homeotropic nematic phase invades the whole sample. The value found in this way closely agrees (within 5%) with that given in Table I.

All the subsequent experiments were carried out at smaller thickness than d_c, contrary to previous experiments with dielectrically positive materials for which $d > d_c$. Experimentally, three intervals of thickness must be considered.

TABLE I. Basic data for the mixtures ZLI 2806 and Roche 2860.

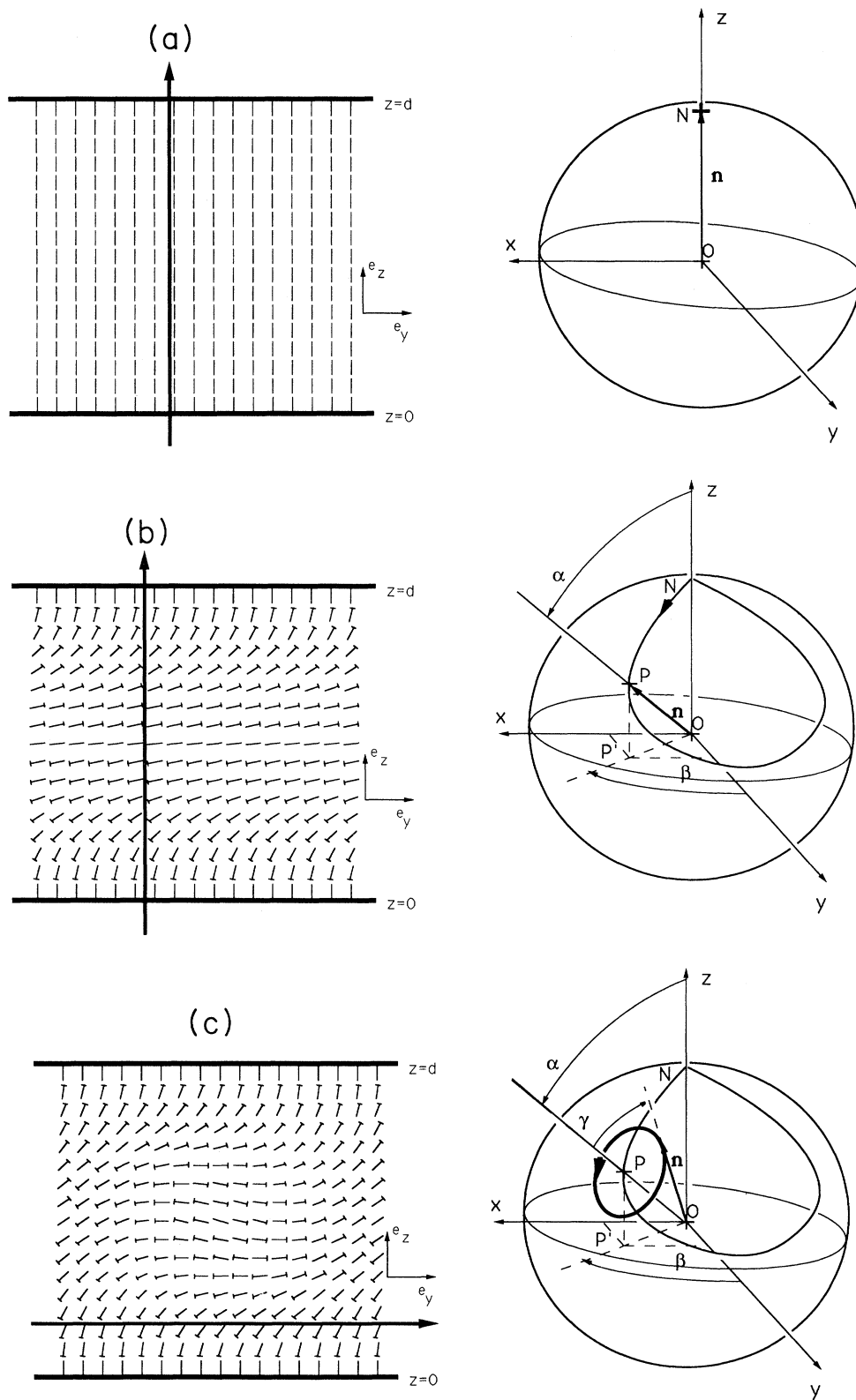| Basic mixture	S811 (wt. %)	Δn	ϵ_a	K_1 (10^{-12} N)	K_2 (10^{-12} N)	K_3 (10^{-12} N)	p (μm)	d_c (μm)
Roche 2860	0.796	0.086	−4.2	15.7	6.63	12.7	16.1	14.3
ZLI 2806	0.792	0.044	−4.8		7.8	15.4	15.7	14.6

FIG. 1. Representation on S^2 (right) and on the real space (left) of various configurations. (a) Homeotropic nematic. The image of a straight line perpendicular to the plates is reduced to the North Pole. (b) Configuration translationally invariant in the (x,y) plane (TIC). The image of a straight line perpendicular to the plates is a closed curve passing through the North Pole. (c) Cholesteric finger parallel to the x axis. The image of a straight line perpendicular to the finger axis and parallel to the plates is a circle whose center is labeled P. The point P describes a curve passing through the North Pole.

(1) For thickness d ranging approximately from $0.7d_c$ to d_c, the phase transition is first order. This can be clearly established by switching on the voltage V from zero and by observing how the texture changes. In this manner, one can distinguish five solutions according to the final value of the voltage, namely the following.

(i) For $V < V_2$, a stable homeotropic nematic phase.

(ii) For $V_2 < V < V_1$, isolated fingers growing from their two ends into the nematic phase [Fig. 2(d)].

(iii) For $V_1 < V < V_0$, a periodic pattern of fingers which grows by forming circular domains (Fig. 3). In order to maintain a constant mean wavelength within each domain, the fingertips split at regular intervals of time. In this region of the phase diagram, the fingers seem to be

200 μm
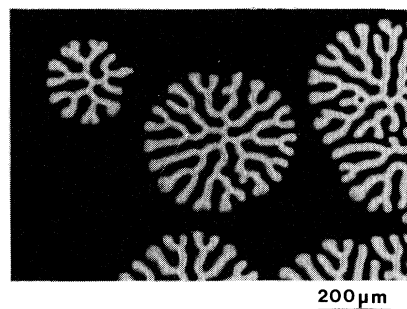
FIG. 3. Circular domains growing in the homeotropic nematic phase. The fingers grow radially and split at their ends in order to maintain a constant wavelength. This growth mode leads to numerous edge dislocations in the periodic pattern of fingers. Mixture ZLI 2806+S811, $V = 0.8$ V, $\mathcal{C} = 0.895$, crossed polarizers.

separated by thin bands of homeotropic nematic phase.

(iv) For $V_0 < V < V_{00}$, a periodic pattern of fingers which develop from a transient spatially homogeneous TIC (Fig. 4). This TIC occurs spontaneously immediately after switching on the voltage (a few hundredths of a second), whereas the subsequent periodic modulation occurs after a much longer relaxation time (a few seconds). Near V_0, the fingers are separated by homeo-
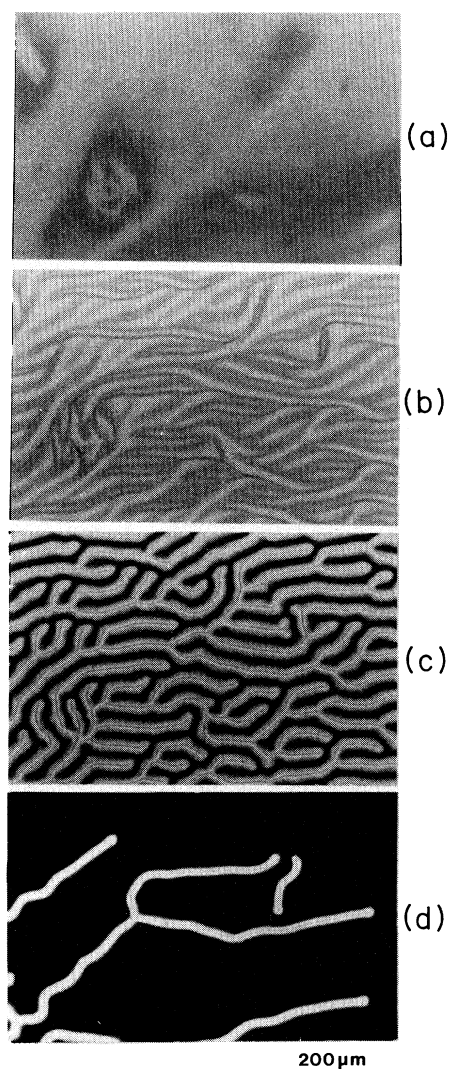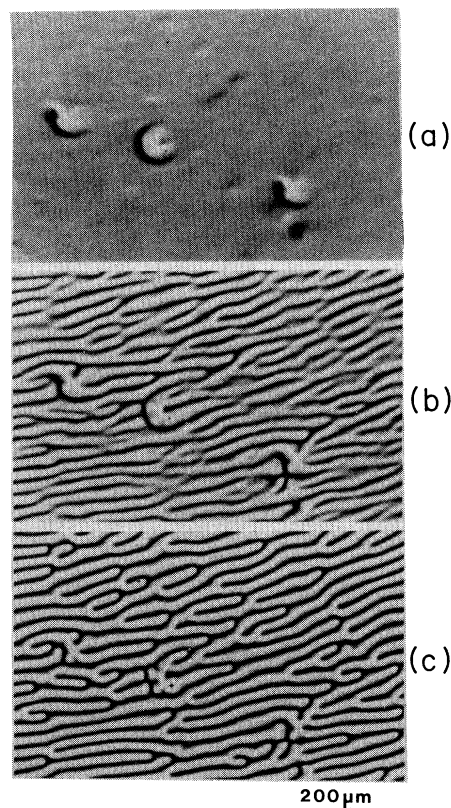

200 μm

FIG. 2. Different textures observed in an electric field in the mixture Roche 2860+S811 between crossed polarizers. (a) TIC developing at high voltage: $V = 2.4$ V, $\mathcal{C} = 0.76$. (b) Periodic structure observed near the transition to the TIC. $V = 2.2$ V, $\mathcal{C} = 0.76$. (c) Periodic pattern of fingers with homeotropic edges. $V = 1.3$ V, $\mathcal{C} = 0.76$. (d) Isolated fingers in coexistence with homeotropic nematic. $V = 0.62$ V, $\mathcal{C} = 0.822$.

200 μm

FIG. 4. Homogeneous development of a transient TIC and its subsequent evolution in ZLI 2806+S811 for $\mathcal{C} = 0.895$, between crossed polarizers; (a) immediately after switching on the voltage (from 0 to 1.2 V); (b) $3s$ later, a periodic modulation occurs; (c) $6s$ later, the system has reached equilibrium.

tropic regions which progressively disappear when one increases the voltage [Figs. 2(c) and 2(b)].

(v) For $V > V_{00}$, the TIC occurs as a whole and remains stable without modulating spatially [Fig. 2(a)].

By decreasing the voltage suddenly from a value V contained between V_2 and V_{00} (finger region) it is possible to define a new limit $V_3 < V_2$ below which the fingers immediately disappear, whereas between V_3 and V_2 the fingers are metastable and slowly shrink by becoming shorter.

The curves $V_i(\mathcal{C})$ ($i = 00, 0, \ldots, 3$) have been graphed on the phase diagrams of both mixtures in Fig. 5. Each line has a clear significance in the language of phase transitions. Thus, V_2 is the critical line on which the nematic and the cholesteric phases coexist. V_3 and V_0 are the spi-

nodal limits of both phases while V_{00} characterizes the finger-TIC transition. Finally, V_1 is the limit between two growth modes of the fingers (either isolated with stable ends or forming a periodic pattern with ends that split easily). Let us now describe what happens at smaller thickness.

(2) For thickness d ranging approximately from $0.55 d_c$ to $0.7 d_c$, the phase transition is second order. Thus, there exists a tricritical point situated at $0.7 d_c$ where all the lines $V_i(\mathcal{C})$ (except V_{00}) converge. In this range of thickness, the nematic state is stable below V_0. Between V_0 and V_{00}, the stable solution is a periodic pattern which always develops in a homogeneous way from a transient TIC. This structure is less regular than before. Its wavelength is large near V_0 and decreases at increasing voltage (Fig. 6). Above V_{00}, the TIC is stable as previously.

(3) Finally, for thickness smaller than $0.55 d_c$, the transition is still second order, with the stable solution above V_0 now replaced by the TIC. One notes that the lines V_0 and V_{00} meet at $d \approx 0.55 d_c$. This particular point is a triple point of the phase diagram, where the nematic phase coexists with both the modulated texture and the TIC. These results are summarized in Fig. 5 where we have plotted the phase diagrams corresponding to ZLI 2806 and Roche 2860.
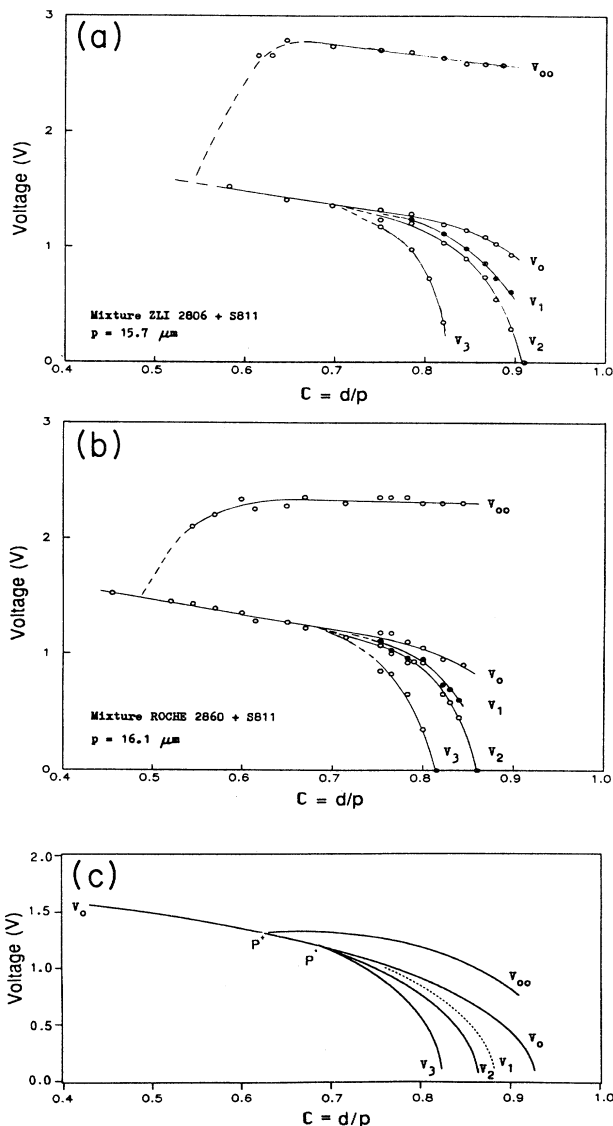

FIG. 5. (a) Experimental phase diagram for ZLI 2806+S811. (b) Experimental phase diagram for Roche 2860+S811. (c) Theoretical phase diagram (calculated with $K_{32} = 1.92$, $K_{12} = 2.37$, and $A = -0.142$).

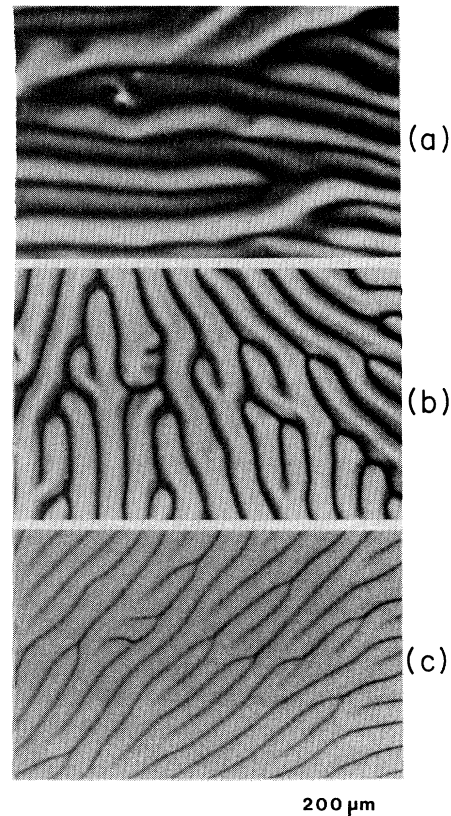FIG. 6. Periodic pattern when the transition is second order (Roche 2860+S811, $\mathcal{C} = 0.65$, crossed polarizers). (a) $V = 1.35$ V. (b) $V = 1.5$ V. (c) $V = 1.9$ V. Note that the wavelength decreases when the voltage increases.

V. THEORETICAL CALCULATION
OF THE PHASE DIAGRAM

In this section we show how to calculate a phase diagram in the $(\mathcal{C}, V)$ plane. We first describe the director field for the TIC. Then, we construct a periodic pattern of fingers by modulating the TIC. Thus, it is possible to pass continuously from one to the other, as is observed experimentally. Then, we calculate the elastic energy, which allows us to predict the transition order. Finally, we draw up the phase diagram.

A. Topological model and nature of the transition

We give first a general expression for the director field which is compatible with the topological considerations of Sec. III.

1. Director field

We assume that the anchoring energy on the electrodes is infinite. Thus, the director $\mathbf{n}$ is parallel to $\mathbf{e}_z$ on the plates at $z = 0$ and d. We denote $Z = \pi z / d$. Any translationally invariant configuration in the horizontal plane can be described by the general director field $\mathbf{n}$,

$$n_x = \sin\alpha(Z)\sin\beta(Z) ,$$
$$n_y = \sin\alpha(Z)\cos\beta(Z) , \qquad (1)$$
$$n_z = \cos\alpha(Z) ,$$

where α is the angle between $\mathbf{n}$ and $\mathbf{e}_z$ and β the angle between the projection of $\mathbf{n}$ in the $(\mathbf{e}_x, \mathbf{e}_y)$ plane and $\mathbf{e}_y$ [Fig. 1(b)].

The experiment shows that the optical contrast of the fingers gradually vanishes when the voltage increases, leading to a TIC. This suggests that the fingers-to-TIC transformation is continuous.

It is possible to construct a periodic pattern of fingers from a TIC by using a mapping to the sphere S^2. We know that the director field $\mathbf{n}_{\text{TIC}}(z)$ is represented by a closed curve on S^2. Let P be a point on this curve corresponding to some value $z = z_0$. In order to modulate this structure in the y direction and to construct a periodic pattern of fingers parallel to the x direction, we transform each point P into a circle of increasing radius. One such circle represents $\mathbf{n}(z_0, y)$ inside a finger. In addition, traversing a single finger in real space is equivalent to going once around this circle in S^2 [Fig. 1(c)]. If all these circles pass through the North Pole (for the same value of y), each finger is bounded by homeotropic nematic phase. The condition of passing through the North Pole is not imposed in the following.

According to this general construction, the coordinates of $\mathbf{n}$ are

$$n_x = \cos\beta \sin\gamma \sin ky - \cos\alpha \sin\beta \sin\gamma \cos ky$$
$$\qquad + \sin\alpha \sin\beta \cos\gamma ,$$
$$n_y = -\sin\beta \sin\gamma \sin ky - \cos\alpha \cos\beta \sin\gamma \cos ky$$
$$\qquad + \sin\alpha \cos\beta \cos\gamma , \qquad (2)$$
$$n_z = \sin\alpha \sin\gamma \cos ky + \cos\alpha \cos\gamma ,$$

where k is the wave vector ($k = 2\pi/\lambda$ and λ is the finger width) and α, β, γ three angles defined in Fig. 1(c).

The homeotropic boundary conditions impose

$$\alpha(Z = 0) = \alpha(Z = \pi) = 0 ,$$
$$\gamma(Z = 0) = \gamma(Z = \pi) = 0 . \qquad (3)$$

One finds again the TIC-director field by putting $\gamma = 0$ in (2), whereas fingers with homeotropic edges correspond to $\alpha = \gamma$.

2. Calculation of the average free energy

In order to calculate the finger free energy, we use the Frank formula

$$f = \tfrac{1}{2}K_1(\nabla \cdot \mathbf{n})^2 + \tfrac{1}{2}K_2(q + \mathbf{n} \cdot \nabla \times \mathbf{n})^2 + \tfrac{1}{2}K_3(\mathbf{n} \wedge \nabla \times \mathbf{n})^2$$
$$\qquad - \frac{\epsilon_a}{2}(\mathbf{E} \cdot \mathbf{n})^2 , \qquad (4)$$

where $q = 2\pi/p$ is the spontaneous twist of the quiescent cholesteric phase and the K_i's are the elastic modulus. We shall neglect the bulk electric field inhomogeneities as well as flexoelectric effects and conduction.

From formulas (2) and (4), one can calculate the average free energy F per unit area in the horizontal plane of the cholesteric. A tedious calculation gives

$$\frac{F}{K_2 q} = \mathcal{C}\left[\left[\frac{k}{q}\right]^2 J - 2\frac{k}{q}\left[I + \frac{H}{2\mathcal{C}}\right] \right] + L + \frac{M + AV^2 N}{\mathcal{C}} , \qquad (5)$$

with

$$\mathcal{C} = \frac{d}{p} = \frac{d}{2}\frac{q}{\pi}$$

and

$$A = \frac{\epsilon_a}{4\pi^2 K_2} .$$

We have

$$H = K_{12}I_{14} + I_{15} + I_{17} + K_{32}(I_{16} + I_{18}),$$
$$I = I_{12} ,$$
$$J = K_{12}(I_1 + I_4) + I_2 + I_5 + K_{32}(I_3 + I_6) ,$$
$$L = I_{13} ,$$
$$M = \tfrac{1}{2}(K_{12}I_7 + I_8 + K_{32}I_9 + I_{10} + K_{32}I_{11}) ,$$
$$N = I_{19} ,$$
$$K_{12} = \frac{K_1}{K_2} ,$$
$$K_{32} = \frac{K_3}{K_2},$$

and

$$I_i = \tfrac{1}{2}\int_0^\pi \mathcal{J}_i dZ .$$

The terms $\mathcal{J}_i$ are listed in Appendix A and depend on α, β, γ and their derivatives with respect to Z, $\dot{\alpha}$, $\dot{\beta}$, and $\dot{\gamma}$.

3. Euler equations: Determination of the spinodal limit of the nematic phase

At equilibrium, the free energy F is minimum. Writing F in the form $F = \frac{1}{2} \int_0^\pi \mathcal{J} \, dZ$ yields the following Euler equations:

$$\frac{\partial \mathcal{J}}{\partial \theta} = \frac{d}{dZ} \frac{\partial \mathcal{J}}{\partial \dot{\theta}} \quad \text{for } \theta \in \{\alpha, \beta, \gamma\} \ . \tag{6}$$

These equations are simple when $\alpha \ll 1$ and $\gamma \ll 1$ and read [from Eqs. (5) and (6)]

$$\dot{\beta} = -\frac{2\mathcal{C}}{K_{32}} \ ,$$

$$\ddot{\alpha} K_{32} = \alpha \left[4AV^2 - \frac{4\mathcal{C}^2}{K_{32}} \right] \ , \tag{7}$$

$$\ddot{\gamma} K_{32} = \gamma \left[4AV^2 + 2\mathcal{C}^2 \left(\frac{k}{q} \right)^2 (1 + K_{12}) - \frac{4\mathcal{C}^2}{K_{32}} \right] \ .$$

This system has a nontrivial solution satisfying the boundary conditions as soon as

$$4AV^2 = -K_{32} + \frac{4\mathcal{C}^2}{K_{32}} \ .$$

This relation defines a critical voltage

$$V_0(\mathcal{C}) = \left[-\frac{K_{32}}{4A} + \frac{\mathcal{C}^2}{K_{32}A} \right]^{1/2} \ , \tag{8}$$

above which the nematic homeotropic state is unstable. Thus, the curve $V = V_0(\mathcal{C})$ represents the spinodal limit of the nematic. In the vicinity of $V = V_0(\mathcal{C})$, $\alpha = \alpha_0 \sin Z$ and $\gamma = \gamma_0 \sin Z$ with $k \to 0$. This means that the finger width diverges near the spinodal line which is also the critical line when the phase transition is second order. Experimentally, we have indeed observed that the wavelength increases near this line when the transition is second order (between $0.55 d_c$ and $0.7 d_c$).

4. Symmetries and development of the free energy as a function of the order parameters

Minimization of the free energy with respect to k gives

$$\frac{F}{K_2 q} = -\mathcal{C} \frac{(I + H/2\mathcal{C})^2}{J} + L + \frac{M + AV^2 N}{\mathcal{C}}$$

$$\text{with } k = q \frac{(I + H/2\mathcal{C})}{J} \ . \tag{9}$$

In order to calculate the amplitude of the solution in the vicinity of the transition, we search for it in the form

$$\alpha = \alpha_0 \sin Z \ ,$$

$$\beta = \frac{2\mathcal{C}}{K_{32}} \left[\frac{\pi}{2} - Z \right] \ , \tag{10}$$

$$\gamma = \gamma_0 \sin Z \ .$$

These functions are solutions of (7). The choice of the constant in the β expression is justified in Appendix B.

We then expand F to fourth order in α_0 and γ_0, which are the two *order parameters* of the transition. Indeed, the nematic phase corresponds to $\alpha_0 = \gamma_0 = 0$ whereas $\alpha_0 \neq 0$, $\gamma_0 \neq 0$ describes fingers, the TIC corresponding to $\alpha_0 \neq 0$, $\gamma_0 = 0$. One notes that $\alpha_0 = 0$ and $\gamma_0 \neq 0$ lead to $k = 0$ [see Eq. (9) and Appendix A], corresponding to a TIC. Furthermore, when $k = 0$, $\mathbf{n}(\alpha, \beta, 0)$ and $\mathbf{n}(0, \beta, \alpha)$ are related to one other by a single rotation around the north-south axis, whence $F(\alpha, \beta, 0) = F(0, \beta, \alpha)$ and both cases $\alpha_0 = 0$ and $\gamma_0 = 0$ represent the same TIC configurations after minimizing in k. We note that the free energy contains only even terms according to Eq. (9). One then obtains to fourth order

$$\frac{F}{K_2 q} = v\alpha_0^2 + v\gamma_0^2 + B\alpha_0^4 + B\gamma_0^4 + C\alpha_0^2 \gamma_0^2 \ . \tag{11}$$

The coefficients v, B, and C only depend on $\mathcal{C}$ and V and on the material constants.

5. Order of the transition and calculation of the tricritical point

The order of the transition can be found from Eq. (11). Since $v = 0$ on the spinodal line $[V = V_0(\mathcal{C})]$, it is determined by the fourth-order terms in (α_0, γ_0). It is easy to see that the transition is first order if $B < 0$ or $C + 2B < 0$ and second order otherwise. More precisely, if $B < 0$, the nematic-to-TIC transition is first order, whereas the transition from nematic to fingers with homeotropic sides $(\alpha_0 = \gamma_0)$ is first order if $C + 2B < 0$.

In addition, we have calculated the coefficients v, B, and C near the spinodal limit $V = V_0(\mathcal{C})$. We find from (9)

$$B = \frac{\pi}{32 \mathcal{C} K_{32}^2} (12\mathcal{C}^2 - 12\mathcal{C}^2 K_{32} + K_{12} K_{32}^2) \ . \tag{12}$$

and

$$C + 2B = -\frac{64 \mathcal{C} K_{32}^6 (-3 - K_{12} + K_{32})^2 \cos^2(\pi\mathcal{C}/K_{32})}{\pi(1 + K_{12})(2\mathcal{C} - 3K_{32})^2(2\mathcal{C} + 3K_{32})^2(2\mathcal{C} - K_{32})^2(2\mathcal{C} + K_{32})^2} + \frac{3\pi}{16 \mathcal{C} K_{32}^2} (12\mathcal{C}^2 - 12\mathcal{C}^2 K_{32} + K_{12} K_{32}^2) \ . \tag{13}$$

One can easily check that $C < 4B$ so that $C + 2B < 0$ when $B < 0$. The transition is consequently first order if $C + 2B < 0$ and second order otherwise. For $C + 2B = 0$, the transition order changes.

By taking the values of the elastic and electric constants given for the nematic mixture Roche 2860, namely $K_{12} = 2.36$ and $K_{32} = 1.91$ (see Table I), one finds a tricritical point for $\mathcal{C} = \mathcal{C}^* = 0.841$. This value is slightly greater than the experimental one ($\mathcal{C}^* \approx 0.7$).

6. Nature of the solution for a second-order phase transition and position of the triple point

In this section we assume that the transition is second order, i.e., $\mathcal{C} < \mathcal{C}^*$. The question is to find which of the solutions, the TIC or the fingers, is more stable. We have looked for the minima of the free energy (11). These are given in Table II.

By comparing the free energies, we see that the fingers solution is more stable if $C < 2B$, whereas the TIC is more stable when $C > 2B$. The triple point is given by writing $C = 2B$. From (12) and (13), one calculates

$$C - 2B = -\frac{64\mathcal{C}K_{32}^6(-3 - K_{12} + K_{32})^2\cos(\pi\mathcal{C}/K_{32})}{\pi(1 + K_{12})(2\mathcal{C} - 3K_{32})^2(2\mathcal{C} + 3K_{32})^2(2\mathcal{C} - K_{32})^2(2\mathcal{C} + K_{32})^2} + \frac{\pi}{16\mathcal{C}K_{32}^2}(12\mathcal{C}^2 - 12\mathcal{C}^2 K_{32} + K_{12}K_{32}^2) .$$

$$(14)$$

We denote by $\mathcal{C}^+$ the solution to this equation. The voltage value at the triple point is given by $V = V_0(\mathcal{C}^+)$ [Eq. (8)]. One can also verify that $C + 2B > 0$ at this point, which ensures that the transition is second order, as assumed a priori at the beginning of this calculation.

For the Roche product and from Table I, one calculates $\mathcal{C}^+ = 0.763$, a value that is larger than the experimental one. In conclusion, we have found theoretically both a tricritical and a triple point in agreement with observations. We could show (but this is cumbersome) that an expansion of α, β, γ at the higher orders does not change Eqs. (13) and (14) giving the triple and the tricritical points.

With reasonable values of elastic constants, one can fit the spinodal line $V = V_0(\mathcal{C})$ and the tricritical point with experimental results. As an example, for $K_{12} = 1.55$ and $K_{32} = 1.88$, the tricritical point is at $\mathcal{C} \approx 0.687$ and the triple point at $\mathcal{C} \approx 0.631$.

B. Theoretical phase diagram

1. Construction

The director field chosen is the same as before [Eq. (2)]. In order to calculate numerically the energy of the various solutions, we have chosen the angles α, β, and γ as follows:

$$\alpha = \alpha_0 \sin Z ,$$

$$\gamma = \gamma_0 \sin Z ,$$

$$\beta\left[\frac{\pi}{2}\right] = 0 , \qquad (15)$$

$$\dot{\beta} = -\frac{2\mathcal{C}K_{32}}{(\sin^2\alpha + K_{32}\cos^2\alpha)(\sin^2\gamma + K_{32}\cos^2\gamma)} .$$

This choice is not completely arbitrary. Indeed, α and γ vanish on the plates ($Z = 0, \pi$), and β respects the following symmetries: $\alpha \leftrightarrow -\alpha$, $\gamma \leftrightarrow -\gamma$, $\alpha \leftrightarrow \alpha + n\pi$, $\gamma \leftrightarrow \gamma + n\pi$. In addition, after minimization with respect to k, one must have $F(\alpha, \beta, 0) = F(0, \beta, \alpha)$. Consequently, the function $\beta(\alpha, \gamma)$ that minimizes F must satisfy equality $\beta(0, \alpha) = \beta(\alpha, 0)$. Finally, the expression chosen for $\dot{\beta}$ reduces to the exact solution of the second Euler equation (6) in the case of the TIC as $\gamma = 0$.

We have then calculated the free energy $F(\alpha_0, \gamma_0)$ when the two order parameters vary from 0 to $\pi/2$. We recall once more that the two particular solutions $\alpha_0 = 0$ (with $k = 0$) and $\gamma_0 = 0$ correspond to the TIC, whereas any solution with $\alpha_0\gamma_0 \neq 0$ describes a periodic pattern of fingers.

The constants K_{12}, K_{32}, and $A = \epsilon_a/4\pi^2 K_2$ have been chosen in order to best fit the experimental data, more precisely the tricritical point and the spinodal line of the nematic phase [$V = V_0(\mathcal{C})$]. The values obtained in this

TABLE II. Different solutions found when the transition is second order. Note that $k = 0$ when $\alpha_0 = 0$ [see Eq. (9) and Appendix A] and that the two TIC's are the same.

α_0	γ_0	Solution	Free energy
0	0	Nematic	0
0 $\pm\sqrt{-\nu/2B}$	$\pm\sqrt{-\nu/2B}$ 0	TIC	$-\nu^2/4B$
$\pm\sqrt{-\nu/(C+2B)}$	$\pm\sqrt{-\nu/(C+2B)}$	Fingers with homeotropic sides	$-\nu^2/(C+2B)$

TABLE III. Comparison of manufacturer data and theoretical values of the mixtures Roche 2860 and ZLI 2806.

Nematic mixture	K_{12}		K_{32}		A (V^{-2})	
	Fit	Manufacturer data	Fit	Manufacturer data	Fit	Manufacturer data
Roche 2860	1.55	2.37	1.88	1.92	−0.149	−0.142
ZLI 2860	1.62		2.26	1.97	−0.116	−0.138

way have been reported in Table III where they are compared with those given in Table I.

2. Results

Let us consider, for example, the case $\mathcal{C} = 0.8$ (Fig. 7). For this value, the phase transition is first order. According to the voltage value, one finds different solutions that can be described as follows.

For $0 \leq V < V_3$ [11] only the homeotropic nematic liquid crystal is stable.

For $V_3 < V < V_2$, another local-energy minimum ap-

FIG. 7. Isoenergy lines (in units of K_2q) as a function of α_0 (x axis) and γ_0 (y axis) for various values of the voltage. α_0 and γ_0 are in the range from 0 to $\pi/2$. The voltage (in volts), the frustration ratio $\mathcal{C}$, and the spacing (in units of K_2q) between two isoenergy lines are given in this order at the top of each graph.

pears, which corresponds to metastable fingers. This zone disappears when the transition is second order.

For $V_2 < V < V_0$, the periodic fingers become more stable than the nematic state, which is still a local minimum.

For $V_0 < V < V_{00}$, the nematic phase is unstable and the fingers are stable.

For $V > V_{00}$, the TIC is stable.

These limits have a clear physical significance. Indeed, the lines $V = V_3$ [11] and $V = V_0$ are, respectively, the spinodal limits of the periodic fingers and of the nematic phase. On the other hand, the line $V = V_2$ is the critical line where the fingers and the nematic phase have the same energy. Finally, the fingers disappear above $V = V_{00}$ and are replaced by a TIC.

So far, we have assumed in our calculations that the fingers form a periodic pattern (called sometimes fingerprint pattern). The experiment shows that isolated fingers, rather than a periodic pattern, grow near the critical line $V = V_2$. As in Ref. [6], one can distinguish theoretically these two kinds of solutions. In particular, it is possible to show that the width of isolated fingers becomes infinite for an intermediate voltage ranging between V_0 and V_2. Experimentally, and for some dynamical reasons that are still unexplained, the periodic pattern occurs when the width of an isolated finger equals roughly 1.4 times the wavelength of the corresponding periodic pattern. This criterion allows us to calculate the line $V = V_1$.

In conclusion, we have all the tools necessary to calculate a phase diagram [11] (Fig. 5). Except for the line V_{00} separating the TIC from the periodic pattern, there is good agreement with experiment. The disagreement concerning this line is perhaps due to inhomogeneities of the electric field in the bulk which are important when the distance to the spinodal line $V = V_0$ is large.

VI. CONCLUSION

We have shown that the phase diagram of a dielectrically negative cholesteric liquid crystal sandwiched between two glass plates with homeotropic anchoring had a Landau tricritical point and a triple point. By generalizing the model of Ref. [6] with two order parameters α_0 and γ_0, we were able to explain the general properties of this phase diagram and to calculate analytically the coordinates in the $(\mathcal{C}, V)$ plane of these two special points. One of the major advantages of this model is to permit a rigorous calculation of the director trajectory on S^2 for
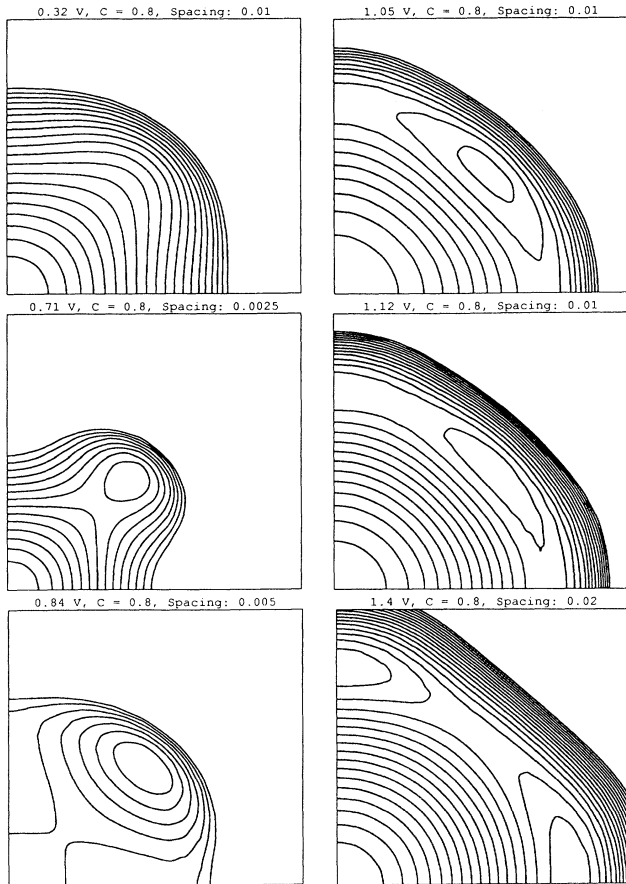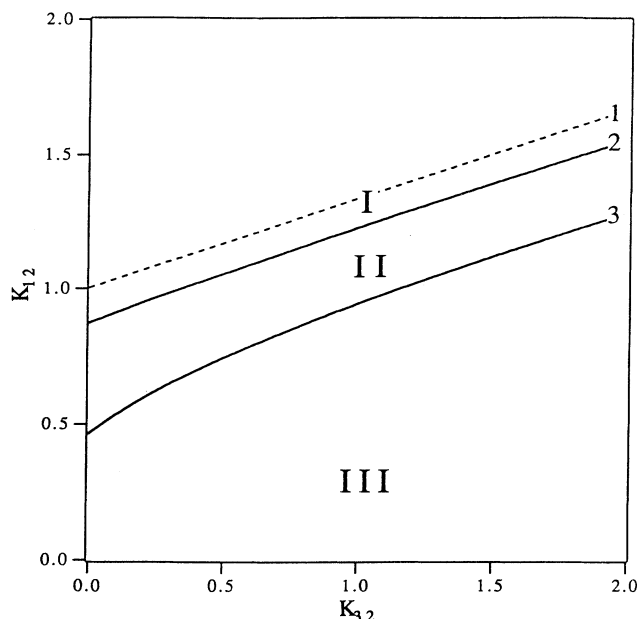
FIG. 8. Lines in parameter space of elasticity constants separating regions of different nature. In region I the transition is first order and the fingers are more stable than the TIC. In region II it is second order with fingers, whereas it is second order with TIC in region III. For the significance of the different lines, see text.

the TIC. In particular, we no longer assume that this trajectory is a circle passing through the North Pole (as assumed in Ref. [6]). On the contrary, we show that the real curve has, in general, an angular discontinuity at the North Pole that is characterized by the difference $\beta(\pi)-\beta(0)$, which depends on the chirality of the liquid crystal.

It is also possible to use this more rigorous model for establishing the theoretical phase diagram of materials with positive dielectric anisotropy at $d > d_c$. One can show that the results found in this way are not very different from those found previously and that the phase diagram is qualitatively unchanged.

One can also calculate analytically, at zero electric field, the demarcation curves of regions in parameter space (K_{12}, K_{32}) of elastic constants where the nematic-cholesteric transition is first or second order. These results are summarized in Fig. 8. Three curves must be considered: curve 1,

$$K_{32} = \tfrac{1}{3} K_{12} + 1 \; ;$$

curve 2,

$$K_{32} = -15 - 17K_{12} + 2(63 + 138K_{12} + 75K_{12}^2)^{1/2} \; ;$$

curve 3,

$$K_{32} = -3 - 5K_{12} + 2(3 + 10K_{12} + 7K_{12}^2)^{1/2} \; .$$

These express the conditions $B = 0$, $C + 2B = 0$, and $C - 2B = 0$, respectively.

Curve 1 has already been calculated in Ref. [9]. Below this line the nematic-TIC transition is second order, whereas it is first order above. On the other hand, curve 2 is the curve below which the nematic-finger transition is second order and above which it is first order. This curve was calculated numerically in Ref. [9] with an approximate model and was found to be slightly shifted with respect to the exact result given here. Finally, curve 3 allows us to compare the energy of the TIC and the fingers. Below this curve, the TIC is more stable than the fingers, whereas the contrary is true above. This result is strictly valid only as the transition is second order, but we expect it to be true also when the transition is first order (a numerical calculation has confirmed this result). One can thus divide the (K_{32}, K_{12}) plane into essentially three regions. Below curve 3 (region III), the transition is second order and the TIC is the most stable solution. One can show that, in this region, the TIC occurs at $\mathcal{C} = K_{32}/2$ and is represented near to the transition by a circle tangent to the North Pole on S^2 which is swept out at constant velocity. Between curves 3 and 2 (region II), the transition is second order but the fingers are now more favorable energetically than the TIC. Finally, above curve 2 (region I), the transition is first order with fingers.

In the future, it would be important to explain why curve $V = V_{00}$ is so different experimentally and theoretically. Two physical phenomena may play an important role: the anchoring energy of the molecules on the substrate that we assumed to be infinite in our calculations and the local distortions of the electric field in the bulk of the sample which must be important as one moves away from the spinodal line $V = V_0$. One way to know whether distortions of the electric field are pertinent in explaining this disagreement would be to use a material with a very small dielectric anisotropy. Such an experiment is currently in progress. Finally, we plan to study the dynamics of these patterns and in particular the TIC-finger transformation beyond the spinodal line $V = V_0$, by using our two-order-parameter model.

ACKNOWLEDGMENTS

APPENDIX A: TERMS $\mathcal{J}_i$ APPEARING IN THE FREE ENERGY OF FINGERS

$$\mathcal{J}_1 = \sin^2\gamma \cos^2\alpha \; ,$$

$$\mathcal{J}_2 = \sin^2\gamma \cos^2\gamma + 2 \sin^2\alpha - 5 \cos^2\gamma \sin^2\alpha + 3 \cos^4\gamma \sin^2\alpha \; ,$$

$$\mathcal{J}_3 = \sin^4\gamma - \sin^2\alpha + 4\sin^2\alpha\cos^2\gamma - 3\cos^4\gamma\sin^2\alpha \ ,$$

$$\mathcal{J}_4 = \sin^2\beta\sin^2\alpha\sin^2\gamma \ ,$$

$$\mathcal{J}_5 = \sin^2\beta\sin^2\alpha(-2 + 5\cos^2\gamma - 3\cos^4\gamma) \ ,$$

$$\mathcal{J}_6 = \sin^2\beta\sin^2\alpha(1 - 4\cos^2\gamma + 3\cos^4\gamma) \ ,$$

$$\mathcal{J}_7 = \tfrac{1}{2}[\dot\alpha^2(\cos^2\alpha + 2\cos^2\gamma - 3\cos^2\alpha\cos^2\gamma) + 6\dot\alpha\dot\gamma\sin\alpha\cos\alpha\sin\gamma\cos\gamma + \dot\gamma^2(2\cos^2\alpha + \cos^2\gamma - 3\cos^2\alpha\cos^2\gamma)] \ ,$$

$$\mathcal{J}_8 = \dot\alpha^2(\tfrac{1}{8} - \tfrac{1}{8}\cos^2\alpha - \tfrac{1}{4}\cos^2\gamma + \tfrac{3}{4}\cos^2\gamma\cos^2\alpha + \tfrac{1}{8}\cos^4\gamma - \tfrac{5}{8}\cos^4\gamma\cos^2\alpha) - \dot\alpha\dot\gamma\sin\alpha\cos\alpha\sin\gamma\cos\gamma + \tfrac{1}{2}\dot\gamma^2\sin^2\alpha \ ,$$

$$\mathcal{J}_9 = \dot\alpha^2(\tfrac{3}{8} - \tfrac{3}{8}\cos^2\alpha - \tfrac{1}{4}\cos^2\gamma + \tfrac{3}{4}\cos^2\gamma\cos^2\alpha - \tfrac{1}{8}\cos^4\gamma + \tfrac{5}{8}\cos^4\gamma\cos^2\alpha) - 2\dot\alpha\dot\gamma\sin\alpha\cos\alpha\sin\gamma\cos\gamma$$
$$+ \tfrac{1}{2}\dot\gamma^2(\sin^2\alpha - \cos^2\gamma + 3\cos^2\gamma\cos^2\alpha) \ ,$$

$$\mathcal{J}_{10} = \dot\beta^2(\tfrac{3}{8} + \tfrac{1}{4}\cos^2\alpha + \tfrac{3}{8}\cos^4\alpha + \tfrac{1}{4}\cos^2\gamma + \tfrac{1}{2}\cos^2\gamma\cos^2\alpha - \tfrac{15}{4}\cos^2\gamma\cos^4\alpha + \tfrac{3}{8}\cos^4\gamma - \tfrac{15}{4}\cos^4\gamma\cos^2\alpha + \tfrac{35}{8}\cos^4\alpha\cos^4\gamma) \ ,$$

$$\mathcal{J}_{11} = \dot\beta^2(\tfrac{1}{8} + \tfrac{1}{4}\cos^2\alpha - \tfrac{3}{8}\cos^4\alpha + \tfrac{1}{4}\cos^2\gamma - 3\cos^2\gamma\cos^2\alpha + \tfrac{15}{4}\cos^2\gamma\cos^4\alpha - \tfrac{3}{8}\cos^4\gamma + \tfrac{15}{4}\cos^4\gamma\cos^2\alpha - \tfrac{35}{8}\cos^4\alpha\cos^4\gamma) \ ,$$

$$\mathcal{J}_{12} = 2\cos\beta\sin\alpha\sin^2\gamma \ ,$$

$$\mathcal{J}_{13} = \dot\beta(1 + \cos^2\alpha + \cos^2\gamma - 3\cos^2\alpha\cos^2\gamma) \ ,$$

$$\mathcal{J}_{14} = (\dot\alpha\cos\alpha\sin^2\gamma + \dot\gamma\sin\alpha\sin\gamma\cos\gamma)\sin\beta \ ,$$

$$\mathcal{J}_{15} = (-\dot\alpha\cos\alpha\sin^2\gamma\cos^2\gamma + \dot\gamma\sin\alpha\sin\gamma\cos\gamma)\sin\beta \ ,$$

$$\mathcal{J}_{16} = \dot\alpha\sin\beta\cos\alpha\cos^2\gamma\sin^2\gamma \ ,$$

$$\mathcal{J}_{17} = \dot\beta\sin\alpha\cos\beta(1 + \cos^2\alpha - 6\cos^2\alpha\cos^2\gamma - \cos^4\gamma + 5\cos^4\gamma\cos^2\alpha) \ ,$$

$$\mathcal{J}_{18} = \dot\beta\sin\alpha\cos\beta(-\cos^2\alpha - \cos^2\gamma + 6\cos^2\alpha\cos^2\gamma + \cos^4\gamma - 5\cos^4\gamma\cos^2\alpha) \ ,$$

$$\mathcal{J}_{19} = 2 - 2\cos^2\alpha\cos^2\gamma - \sin^2\alpha\sin^2\gamma \ .$$

APPENDIX B: CALCULATION OF $\beta(\pi/2)$ NEAR THE SPINODAL LINE

The system of Eqs. (2) does not define entirely β, since it is necessary to calculate the constant term $b = \beta(\pi/2)$. Equation (9) gives

$$F(\alpha,\dot\beta,\gamma,b) = \frac{-\mathcal{C}\left[I(\alpha,\dot\beta,\gamma,b) + \dfrac{H(\alpha,\dot\beta,\gamma,b)}{2\mathcal{C}}\right]^2}{J(\alpha,\dot\beta,\gamma,b)}$$
$$[+f(\alpha,\dot\beta,\gamma)] \ .$$

For a second-order transition, $\alpha \ll 1$ and $\beta \ll 1$ in the vicinity of the transition, and J does not depend on b to be second order in (α,γ). Thus at lowest order, J does not depend on b and F is proportional to $(I + H/2\mathcal{C})^2$.

One can establish that

$$\frac{\partial^2}{\partial b^2}\left[I + \frac{H}{2\mathcal{C}}\right] = -\left[I + \frac{H}{2\mathcal{C}}\right] \ ,$$

thus

$$I + \frac{H}{2\mathcal{C}} = \kappa\cos(b + \varphi) \ .$$

For $b = \pi/2$, the symmetries of $\alpha, \gamma, \dot\beta$,

$$\alpha(\pi - Z) = \alpha(Z) \ ,$$

$$\gamma(\pi - Z) = \gamma(Z) \ ,$$

$$\dot\beta(\pi - Z) = \dot\beta(Z) \ ,$$

give $I = 0$ and $H = 0$. Therefore $\varphi = 0$ and F is minimal for $b = n\pi$, $n \in \mathbb{Z}$. This explains our choice: $b = 0$. The direction of modulation of the TIC is therefore parallel to the horizontal projection of the director **n** in the median plane of the sample, i.e., in the Y direction.

*Permanent address: University of Chemical Technology, 532 10 Pardubice, Czechoslovakia.

[1] M. Brehm, H. Finkelmann, and H. Stegemeyer, Ber. Bunsenges. Phys. Chem. **78**, 883 (1974).

[2] T. Harvey, Mol. Cryst. Liq. Cryst. **34**, 224 (1978).

[3] M. J. Press and A. S. Arrott, J. Phys. (Paris) **37**, 387

(1976).

[4] M. J. Press and A. S. Arrott, Mol. Cryst. Liq. Cryst. **37**, 81 (1976).

[5] A. Stieb, J. Phys. (Paris) **41**, 961 (1980).

[6] P. Ribière and P. Oswald, J. Phys. (Paris) **51**, 1703 (1990).

[7] S. Pirkl, Cryst. Res. Technol. **26**, 371 (1991).

[8] S. Pirkl, Cryst. Res. Technol. **26**, K111 (1991).

[9] F. Lequeux, P. Oswald, and J. Bechhoefer, Phys. Rev. A **40**, 3974 (1989).

[10] F. Lequeux, J. Phys. (Paris) **49**, 967 (1988).

[11] The spinodal limits for isolated fingers and periodic pat-
terns are not exactly identical. In the theoretical phase diagram, we consider the case of isolated fingers because the fingers are separated from each other by homeotropic strips as they disappear.
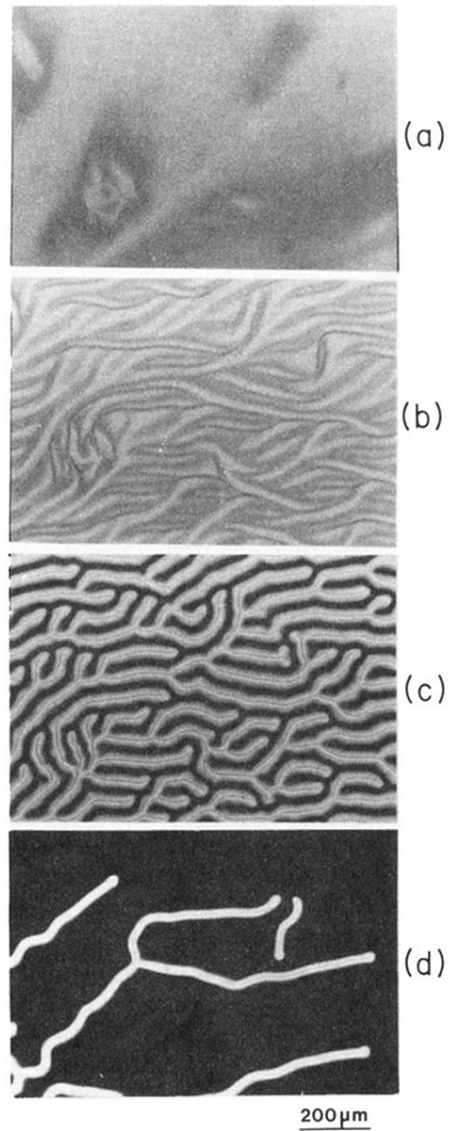
FIG. 2. Different textures observed in an electric field in the mixture Roche 2860+S811 between crossed polarizers. (a) TIC developing at high voltage: $V=2.4$ V, $\mathcal{C}=0.76$. (b) Periodic structure observed near the transition to the TIC. $V=2.2$ V, $\mathcal{C}=0.76$. (c) Periodic pattern of fingers with homeotropic edges. $V=1.3$ V, $\mathcal{C}=0.76$. (d) Isolated fingers in coexistence with homeotropic nematic. $V=0.62$ V, $\mathcal{C}=0.822$.
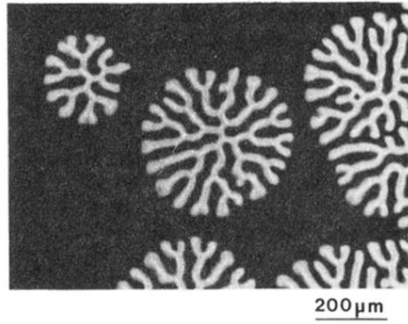
200 μm

FIG. 3. Circular domains growing in the homeotropic nematic phase. The fingers grow radially and split at their ends in order to maintain a constant wavelength. This growth mode leads to numerous edge dislocations in the periodic pattern of fingers. Mixture ZLI 2806+S811, $V = 0.8$ V, $\mathcal{C} = 0.895$, crossed polarizers.
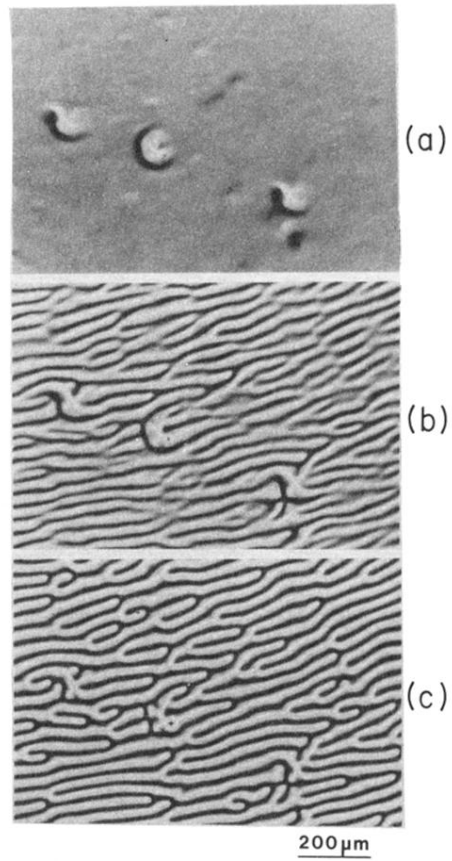
FIG. 4. Homogeneous development of a transient TIC and its subsequent evolution in ZLI 2806+S811 for $\mathcal{C}=0.895$, between crossed polarizers; (a) immediately after switching on the voltage (from 0 to 1.2 V); (b) 3s later, a periodic modulation occurs; (c) 6s later, the system has reached equilibrium.
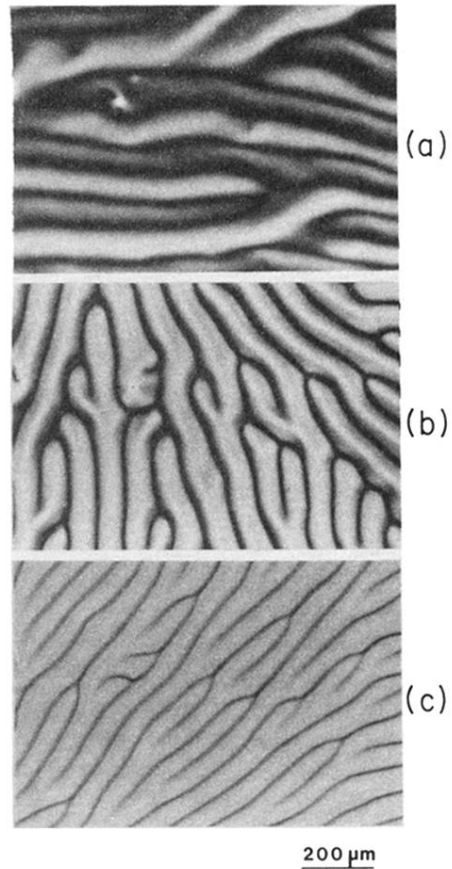
200 μm

FIG. 6. Periodic pattern when the transition is second order (Roche 2860+S811, $\mathcal{C}=0.65$, crossed polarizers). (a) $V=1.35$ V. (b) $V=1.5$ V. (c) $V=1.9$ V. Note that the wavelength decreases when the voltage increases.